Experimentelle Methoden der Teilchenphysik

Sommersemester 2011/2012

Albert-Ludwigs-Universität Freiburg

Prof. Markus Schumacher

Physikalisches Institut, Westbau, 2. OG Raum 008

Telefon 07621 203 7612

E-Mail: Markus.Schumacher@physik.uni-freiburg.de

Kapitel 4: Gasgefüllte Ionisationsdetektoren

http://terascale.physik.uni-freiburg.de/lehre/Sommersemester%202012

A drift chamber is a proportional chamber with additional time measurement:

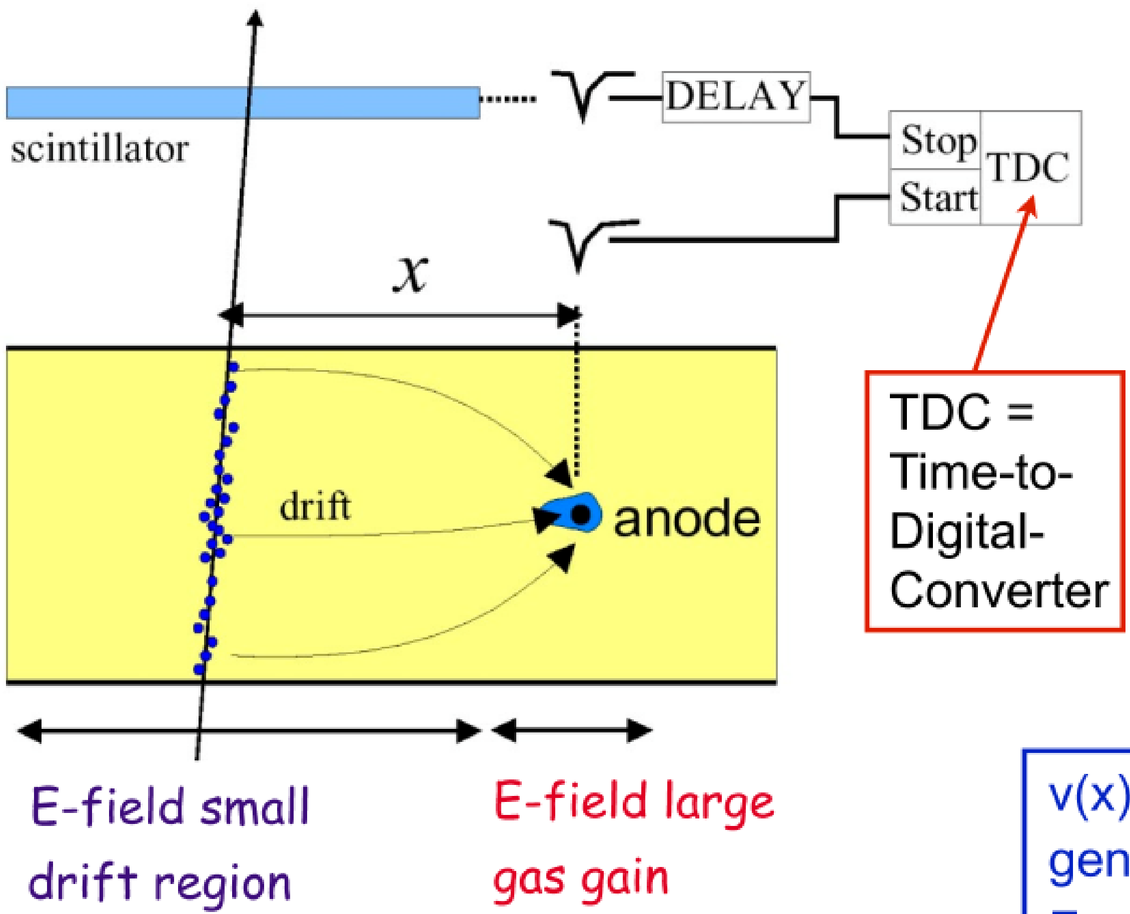

- Need additional detector for start time
- Need to know the drift velocity $v_D(x)$
- Then from $dx/v(x) = dt$
  $\Rightarrow t(x) = \int dx/v(x)$
  $\Rightarrow x(t)$ („space-time relation")
- t measured $\Rightarrow$ distance x from track to anode wire

v(x) depends on $\vec{E}(x)$ and in general has to be calibrated.
For $\vec{E} \approx$ const. $\Rightarrow v(x) \approx$ const. and $x(t) \approx v \cdot t$

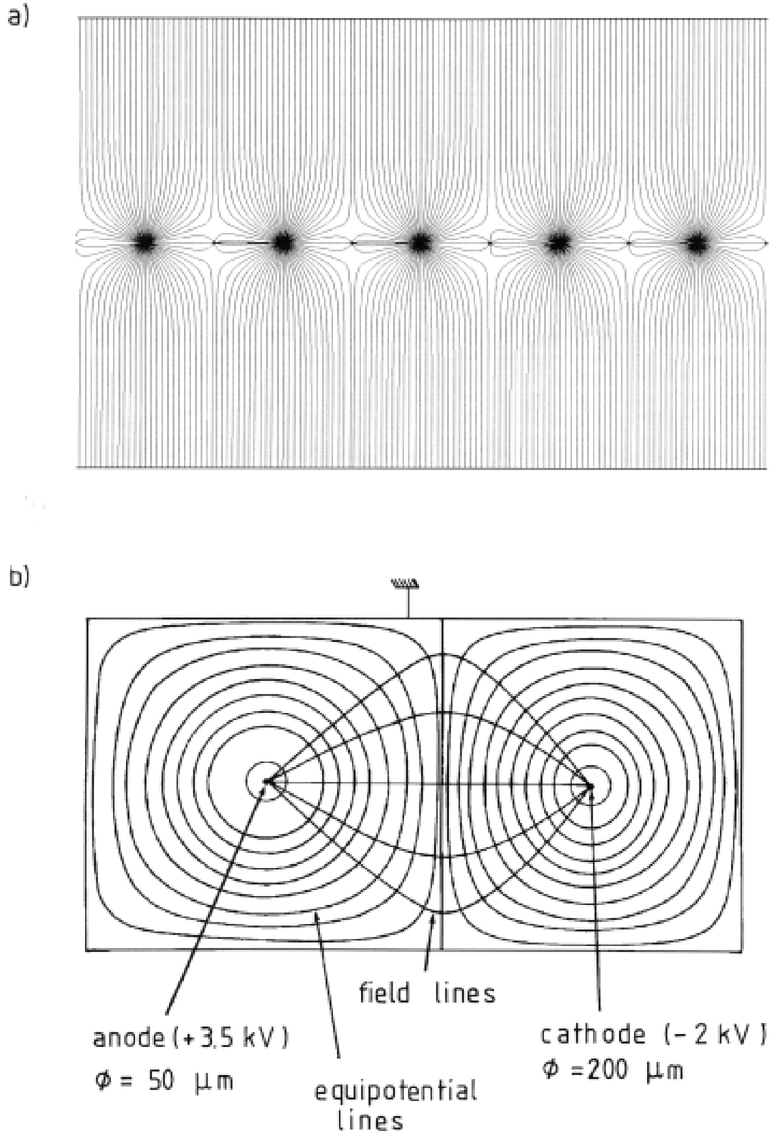

Fig. 4.35. Field lines in a multiwire drift chamber (a) [184] and (b) equipotential and field lines in a multiwire drift chamber cell [51, 224].

- Need „potential wires“ between anode wires to get nearly constant drift field

<u>Advantages (wrt MWPC):</u>

- Number of wires (= number of electronic channels) **reduced**
- Position resolution **improved**
  (1 ns ≈ 50 µm)

Driftkammer: Optimierung der Feldformung

<u>Improvement in field homogeneity:</u>

- by „graded field" (= cathode strips at different potential)

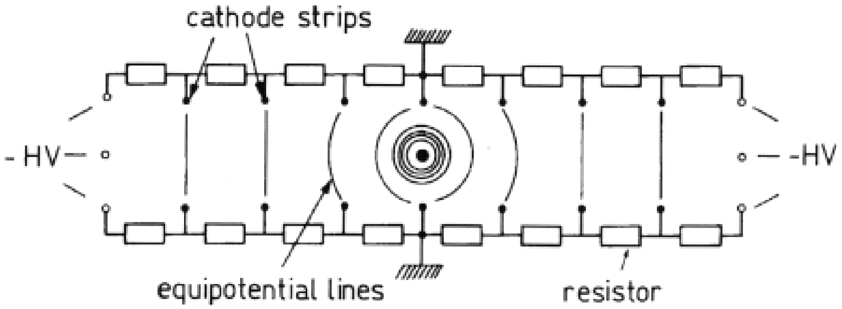

Fig. 4.36. Illustration of the field formation in a large-area drift chamber.

- by electrode-less drift chamber (field formed by ions sticking to insulator)

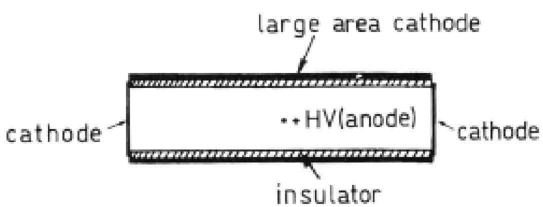

Fig. 4.38. Principle of construction of an electrodeless drift chamber.

Working principle of electrode-less drift chambers:

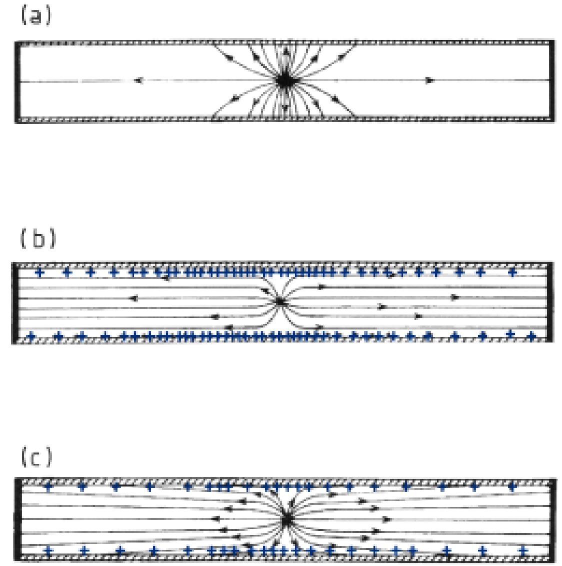

Fig. 4.39. Field formation in an electrodeless drift chamber by ion attachment [228, 229].

<u>Disadvantage:</u> time needed until chamber works, up to hours!

Driftkammer: Beiträge zur Ortsauflösung

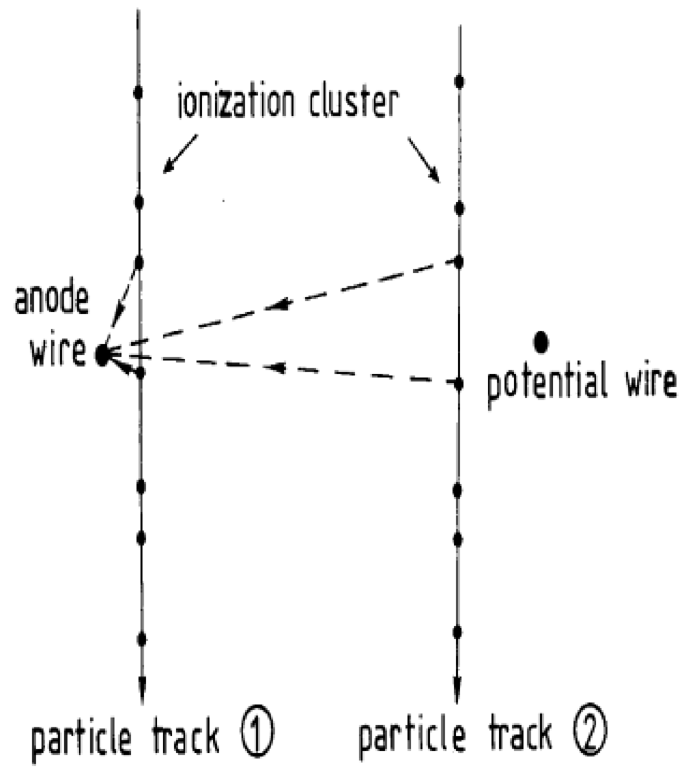

Fig. 4.33. Illustration of different drift paths for 'near' and 'distant' particle tracks to explain the dependence of the spatial resolution on the primary ionization statistics.

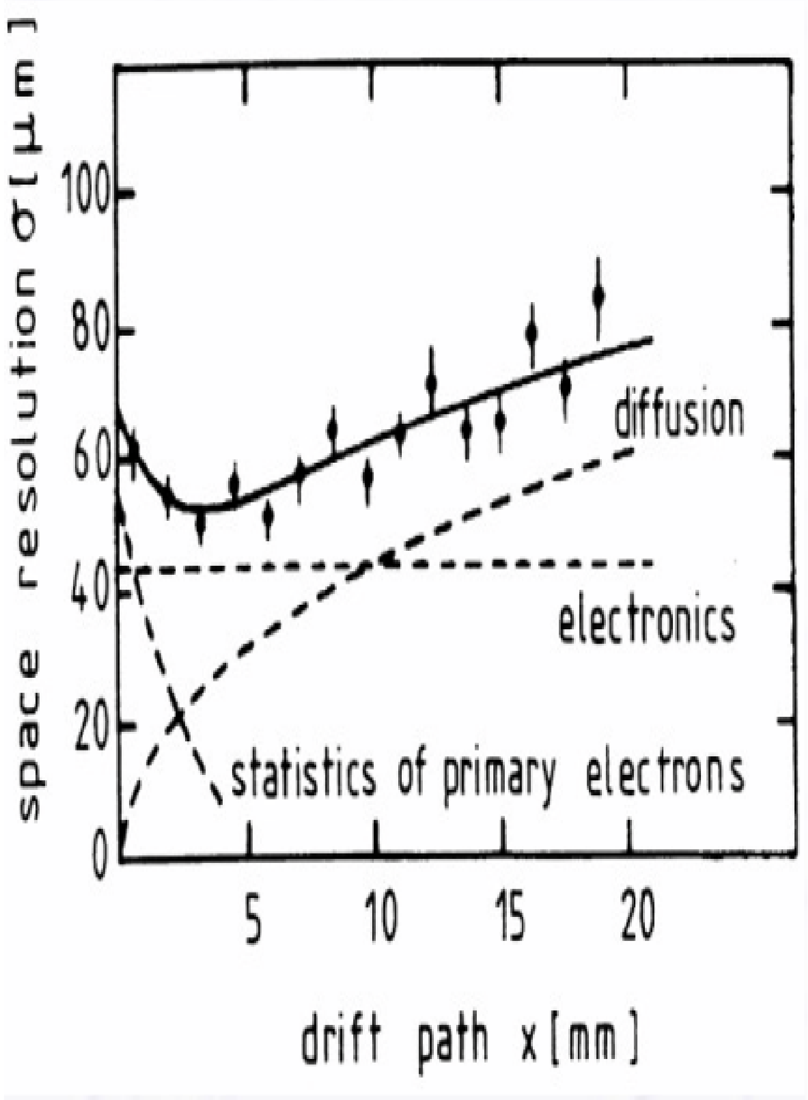

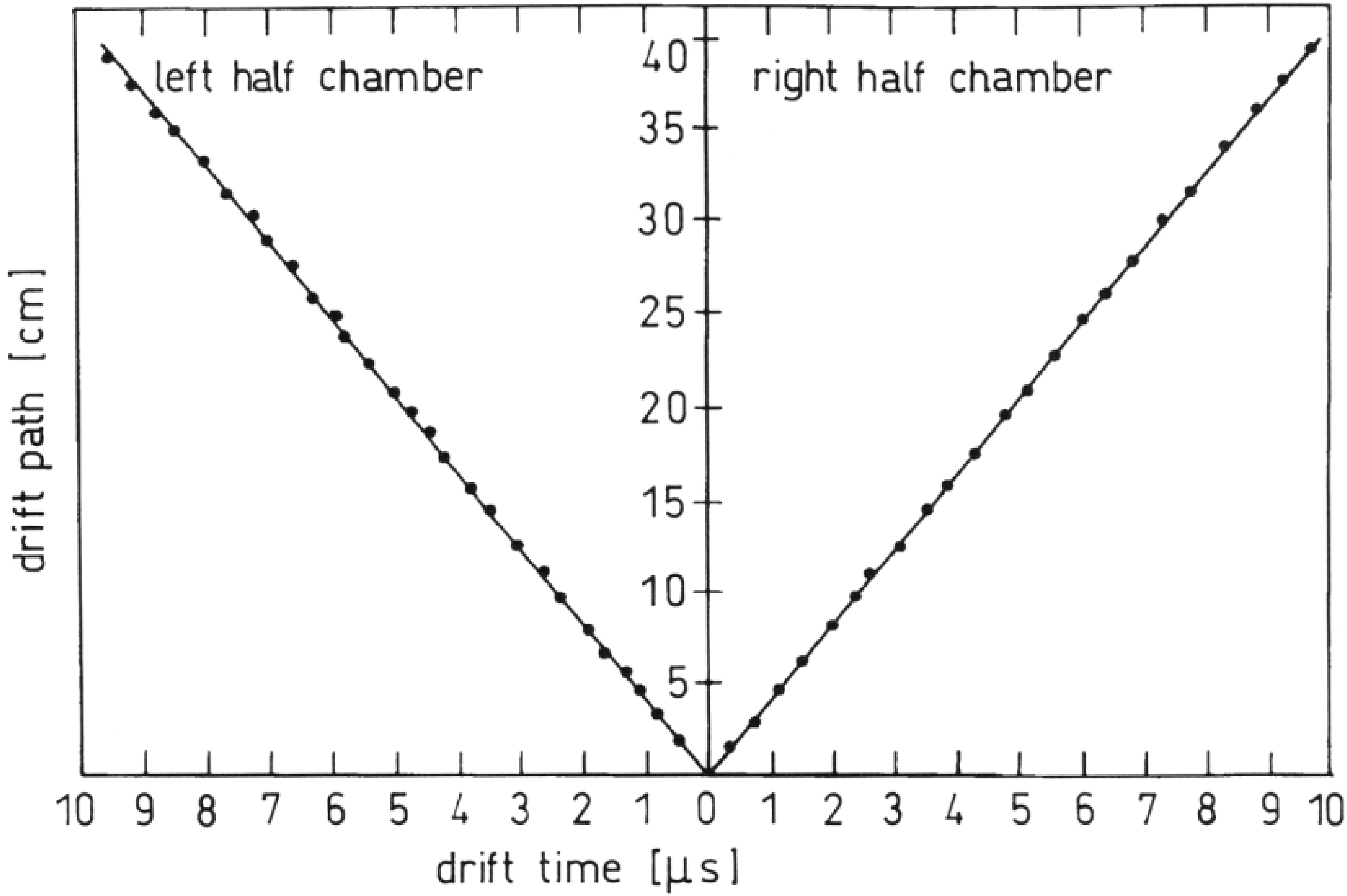

Fig. 4.37. Drift time space relation in a large drift chamber ($80 \times 80\,\mathrm{cm}^2$) with only one anode wire [227].

Zylindrische Driftkammer und Stereodrähte

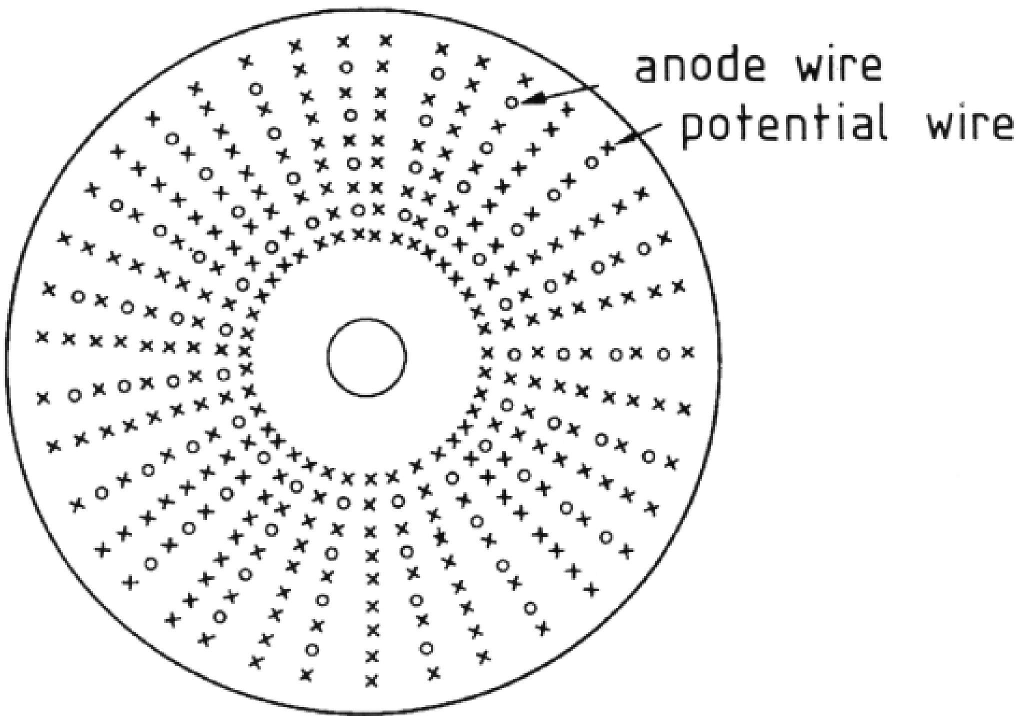

Fig. 4.41. Schematic representation of a cylindrical drift chamber. The figure shows a view of the chamber perpendicular to the wires.

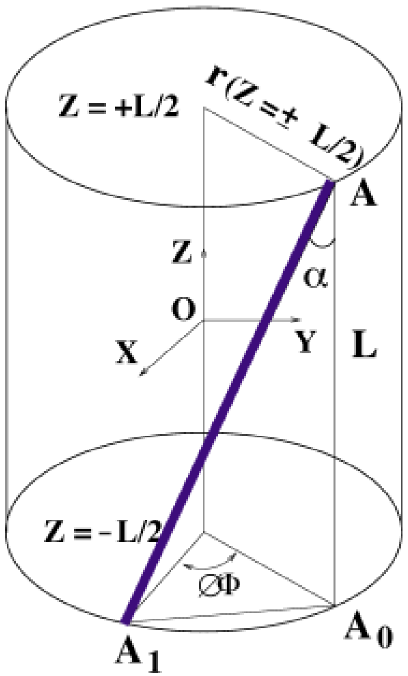

stereo wire for the determination of the second coordinate

Driftzellengeometrien

open geometry

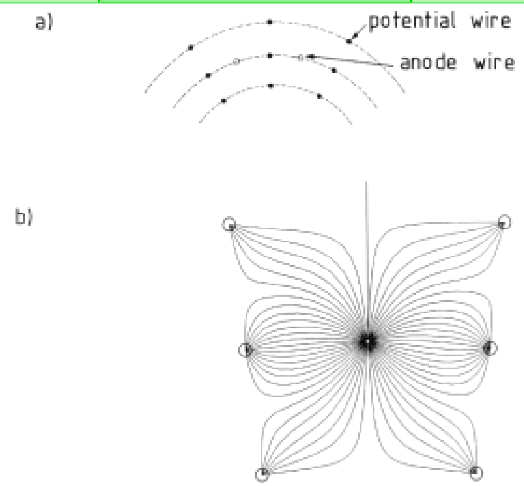

Fig. 4.42. a) Illustration of an open drift cell geometry. b) Field lines in an open drift cell [184].

closed geometry

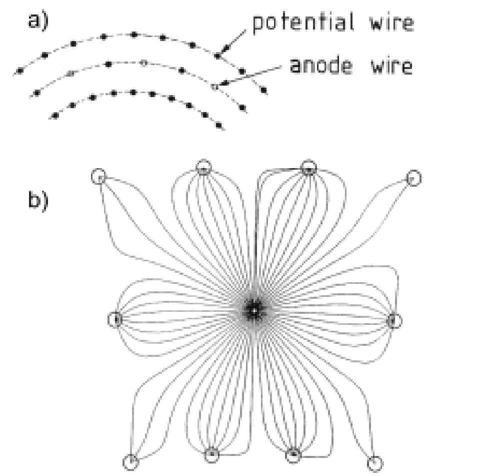

Fig. 4.43. a) Illustration of a closed drift cell geometry. b) Field lines in a closed drift cell [184].

hexagonal geometry

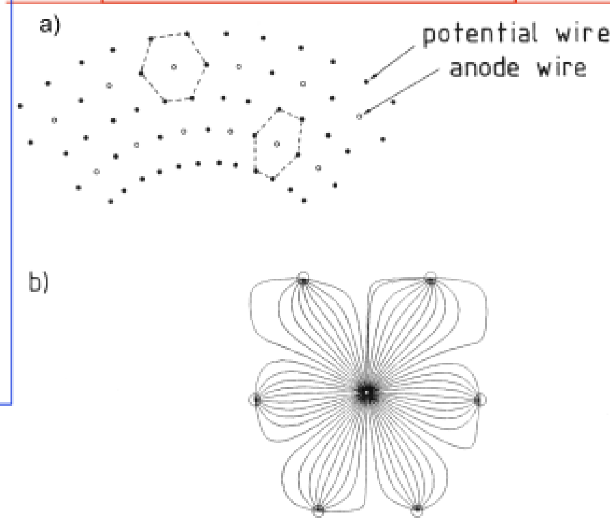

Fig. 4.44. a) Hexagonal drift cell geometry. b) Field lines in a hexagonal drift cell [184].

Signal in einer Jetkammer

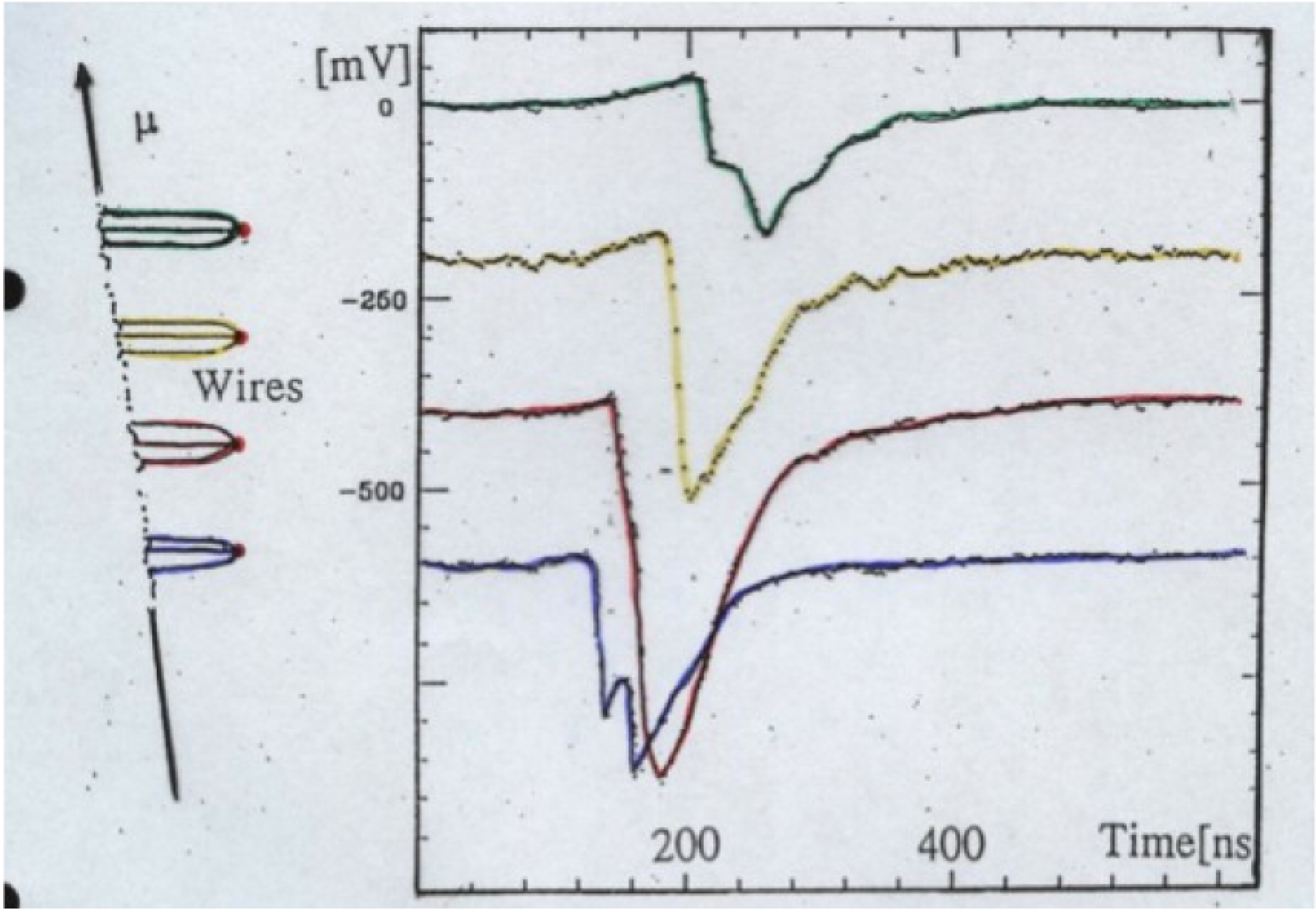

“Staggering” und “Lorentzwinkel”

Example of jet chamber geometry with staggered wires

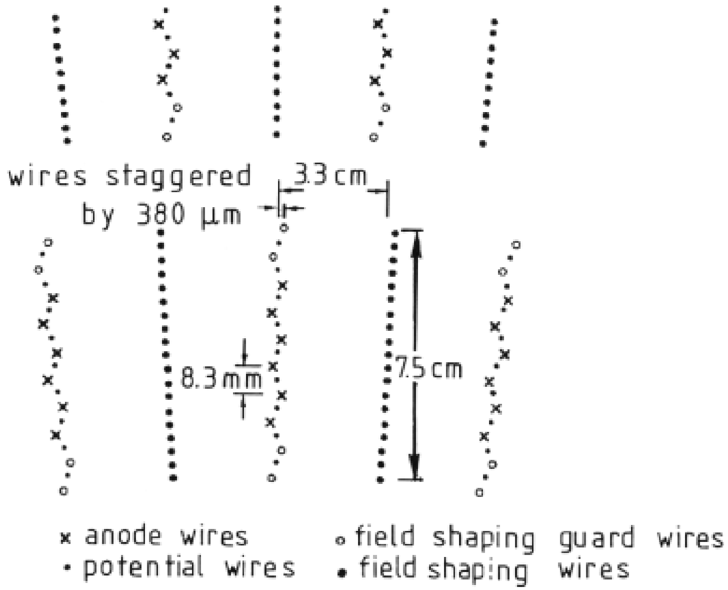

Fig. 4.54. Drift cell geometry of the new MARK II jet drift chamber [265, 266].

Example of the Lorentz angle in a jet chamber geometry

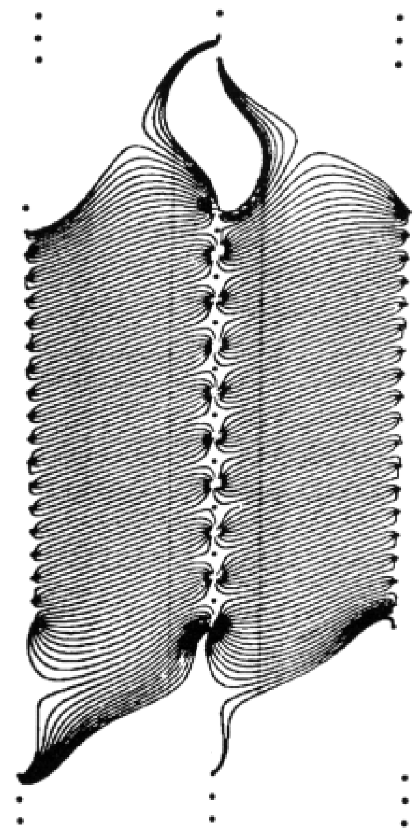

Fig. 4.55. Calculated drift trajectories in a jet chamber drift cell in the presence of a magnetic field [265, 266].

PLUTO at PETRA (DESY)

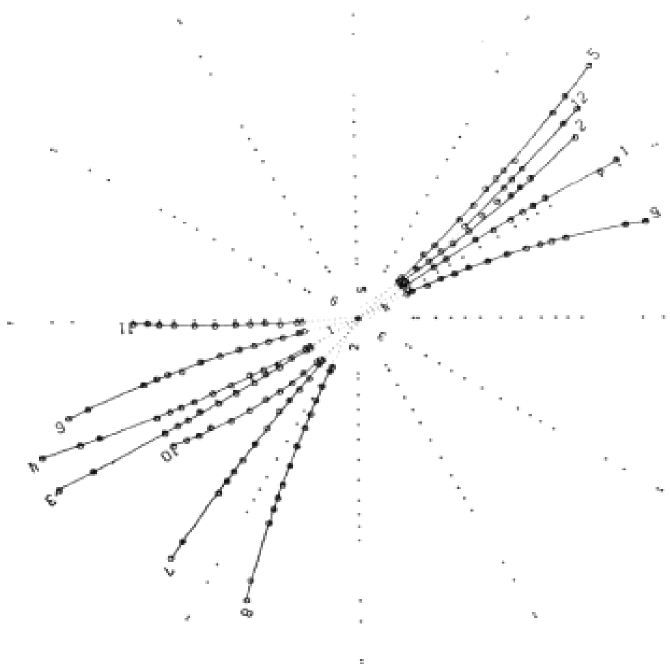

JADE at PETRA (DESY)

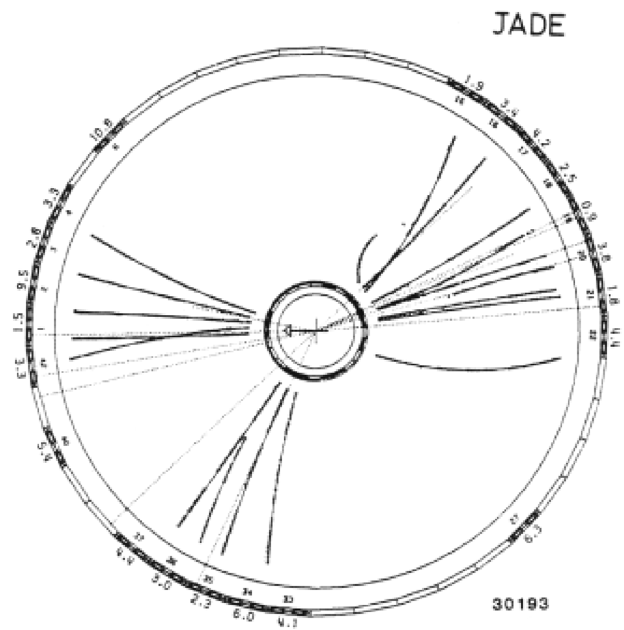

Fig. 4.53. The $r\varphi$ projection of interaction products from an electron-positron collision in the JADE central detector [261, 262, 267]. The bent tracks correspond to charged particles and the dotted tracks to neutral particles which are not affected by the magnetic field (and are not registered in the chamber).

Beispiele

OPAL Central Jet Chamber 1988

(648 sense wires)

H1 Central Jet Chamber

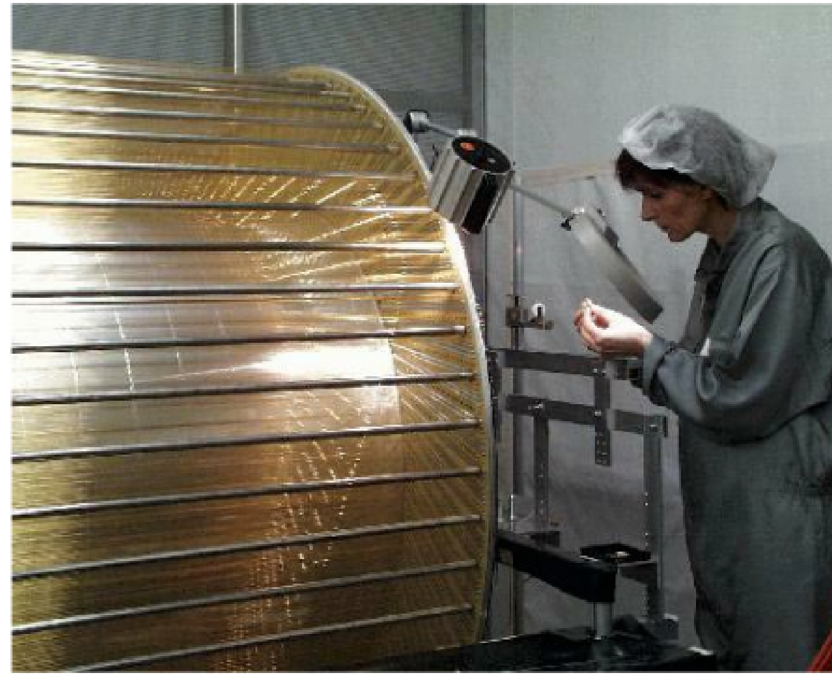

- ≈ 15000 wires
- total force from wire tension ≈ 6 tons

Crossed Planes

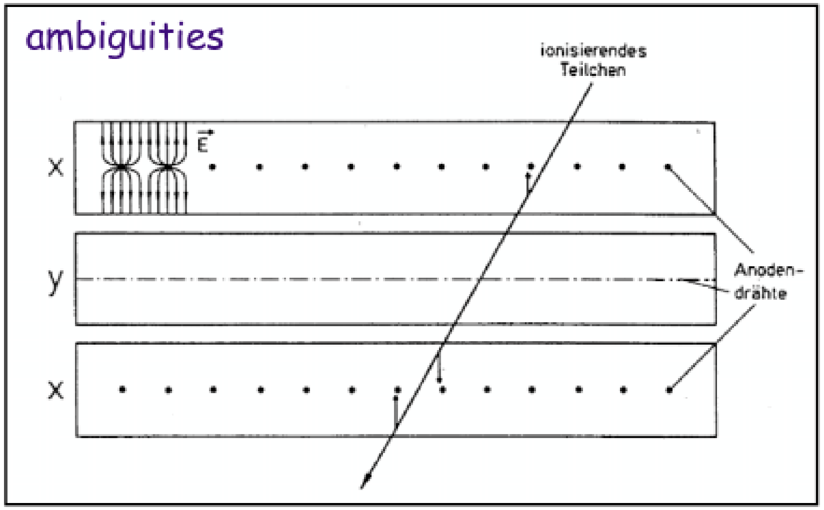

Charge Divison, z-by-timing

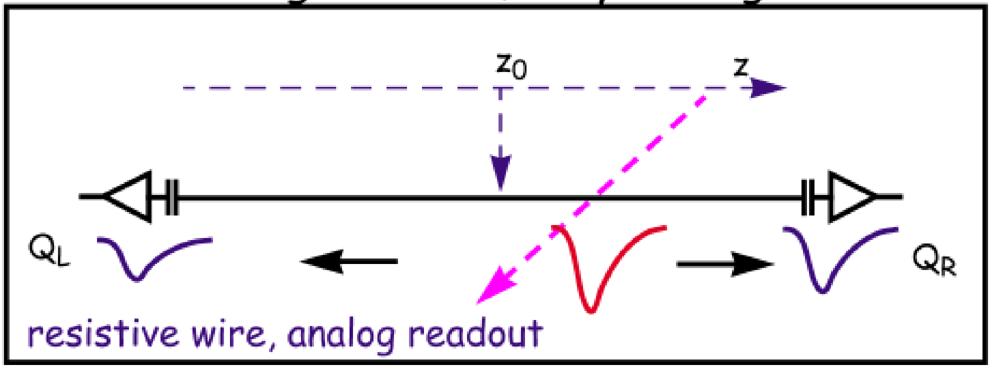

Segmented Cathodes

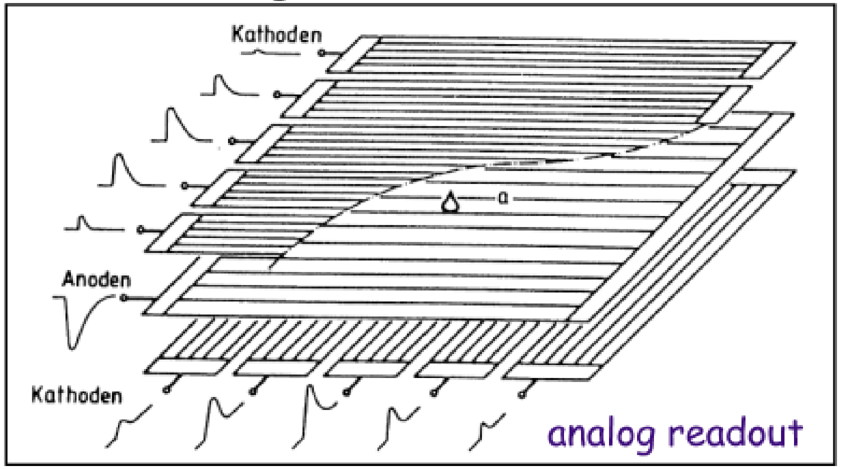

Stereo Wires

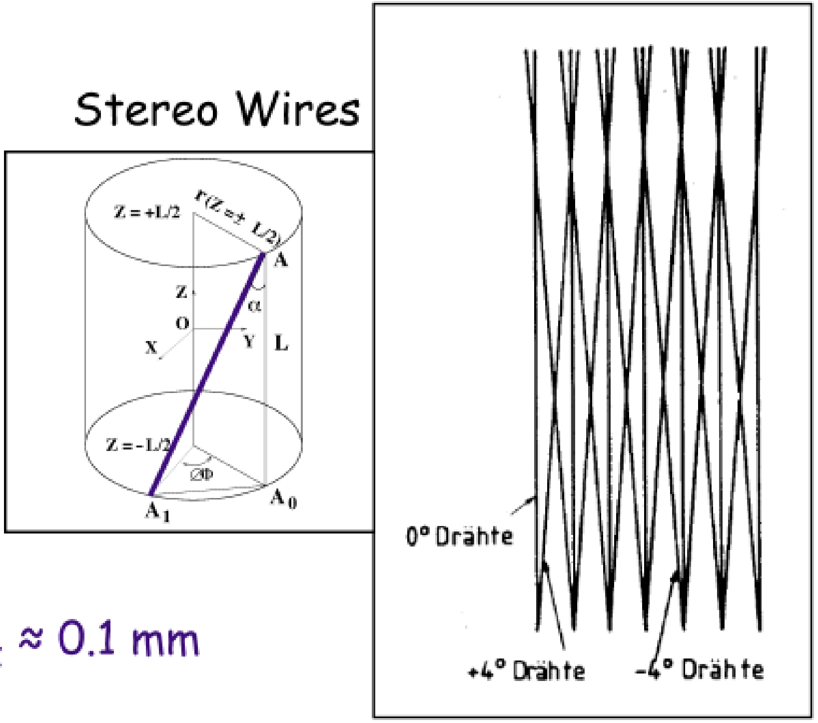

$\rightarrow \sigma_z \approx 0.1$ mm

Zeitprojektionskammer (TPC)

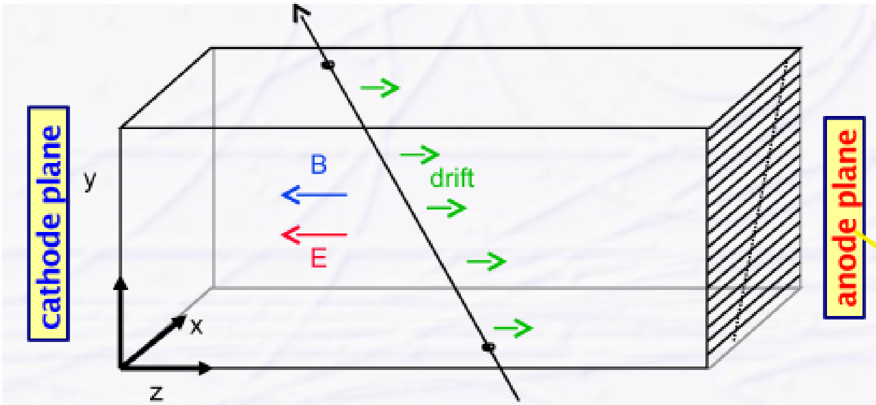

TPC = long drift chamber with $\vec{E} \parallel \vec{B}$

(ALICE TPC: 5m diameter, 5m length)

3D - measurement of tracks

Anode plane is MWPC with
2D coordinate measurement:

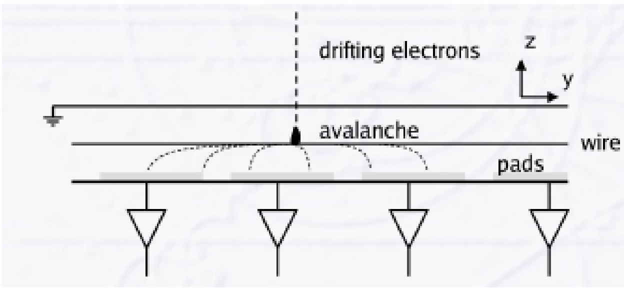

3[rd] coordinate from arrival time of electrons

B-field reduces transverse diffusion:

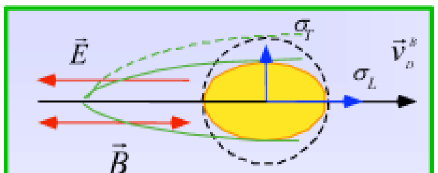

$$\sigma_L = \sigma_0$$

$$\sigma_T = \frac{\sigma_0}{\sqrt{1+\omega^2\tau^2}}$$

$\Rightarrow$

σ_T versus B:

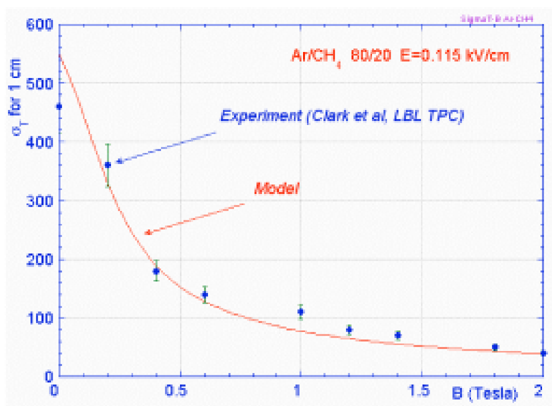

Problem with TPC: positive ions would stay in field volume for a long time

Solution: „Gating“

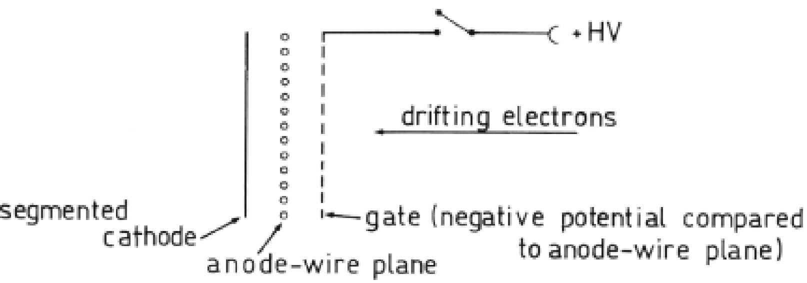

Fig. 4.58. Gating principle in a time projection chamber.

Gate open: very small negative potential wrt. screening grid

Gate closed: large negative potential

Gate open: Gate closed:

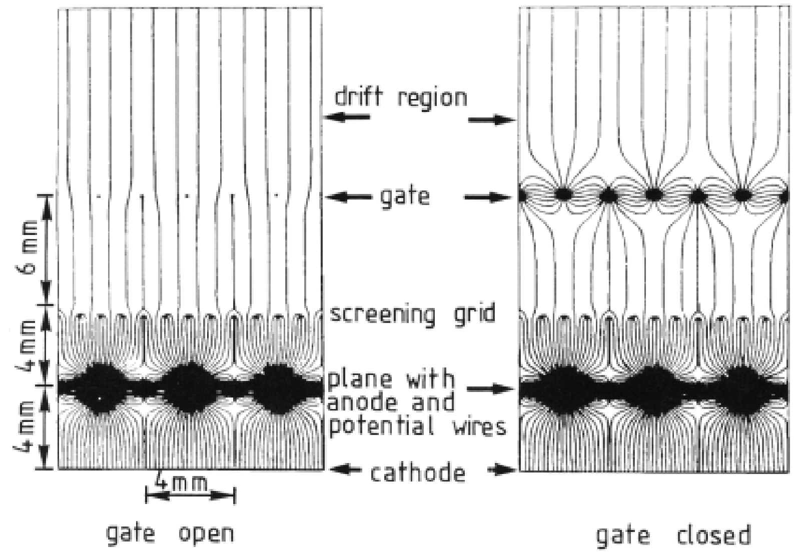

Fig. 4.59. Working principle of the gate in the ALEPH-TPC [270]. For an open gate the ionization electrons are not prevented from entering the gas amplification region. The closed gate, however, confines the positive ions to the gas amplification region. A closed gate also stops electrons in the drift volume from entering the gas amplification region. For an event of interest the gate is first opened to allow the primary electrons to enter the gas amplification region and then it is closed to prevent the positive ions produced in the avalanche process from drifting back into the detector volume.

(from G.Herten)

Problem:
- Ions drift back to central electrode
- Disturbs homogeneity of electric field in drift region.

Solution:
- ions are collected on shielding grid
- only electrons from triggered events reach amplification region, others are collected at gating grid.
- external trigger required.

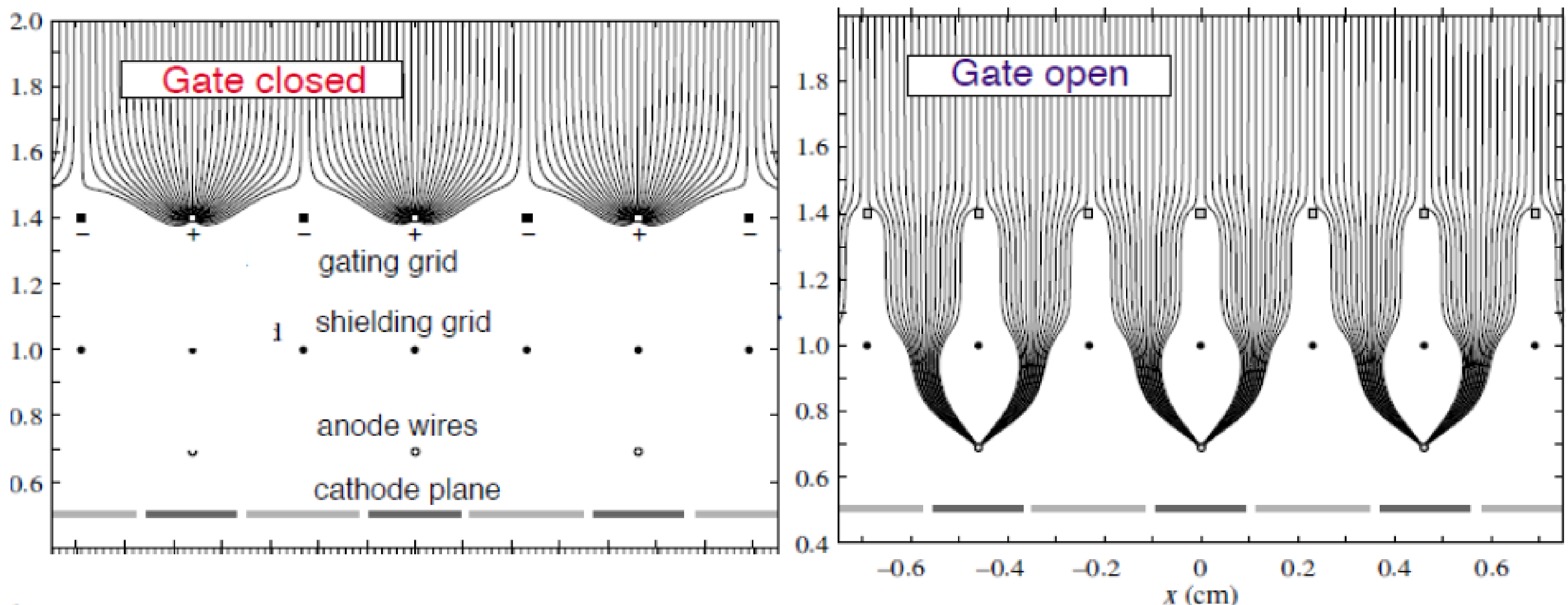

DELPHI TPC

6 sectors in each endcap, each has:
- 16 pad rows (1680 pads) → position determination
- 192 sense wires → dE/dx measurement

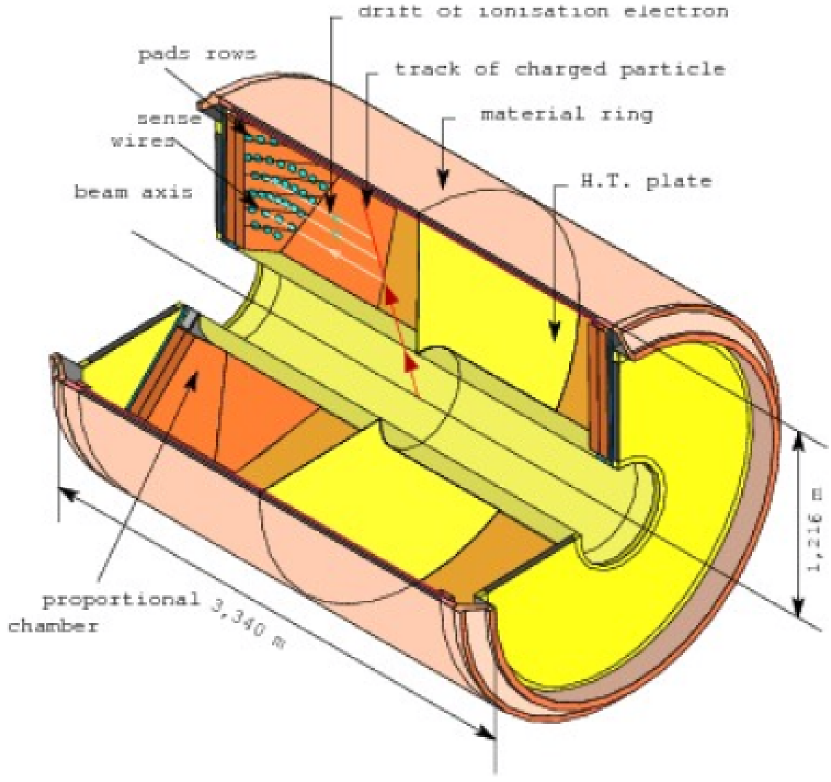

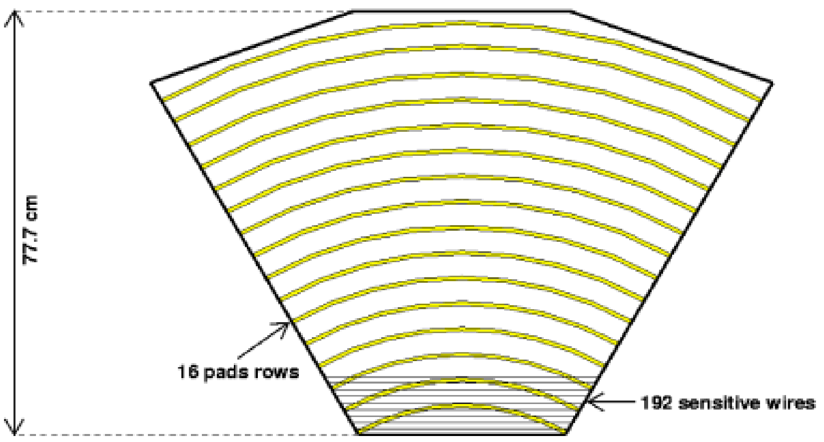

ALEPH TPC

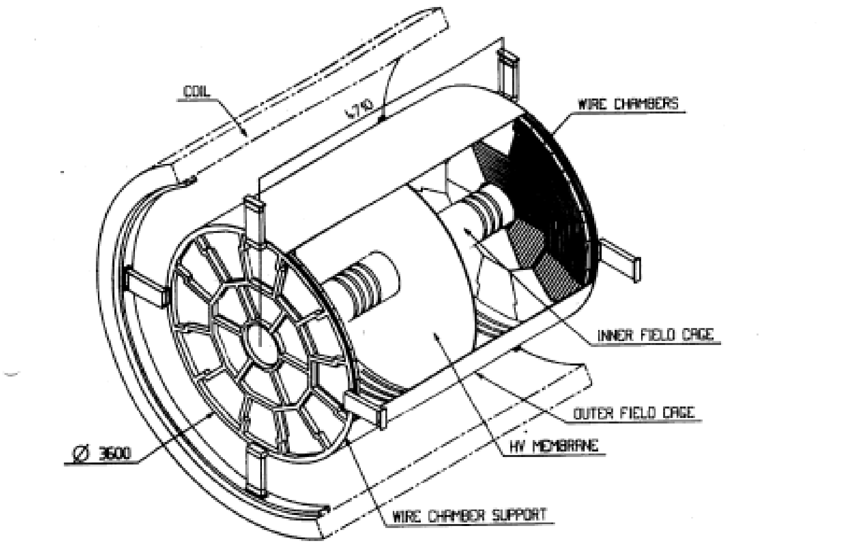

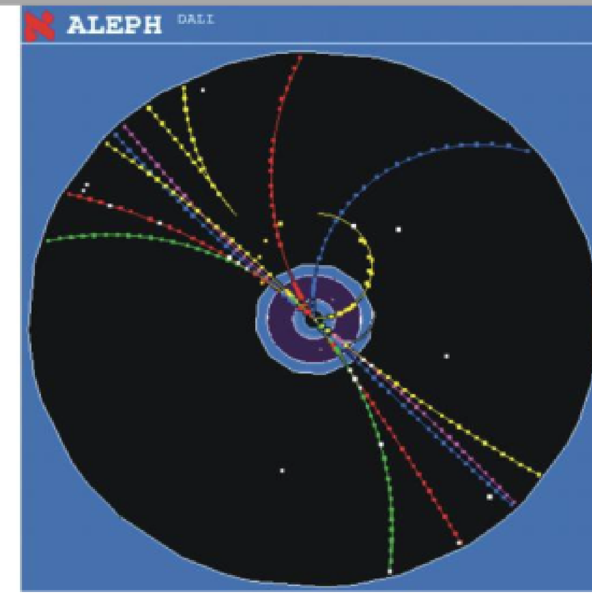

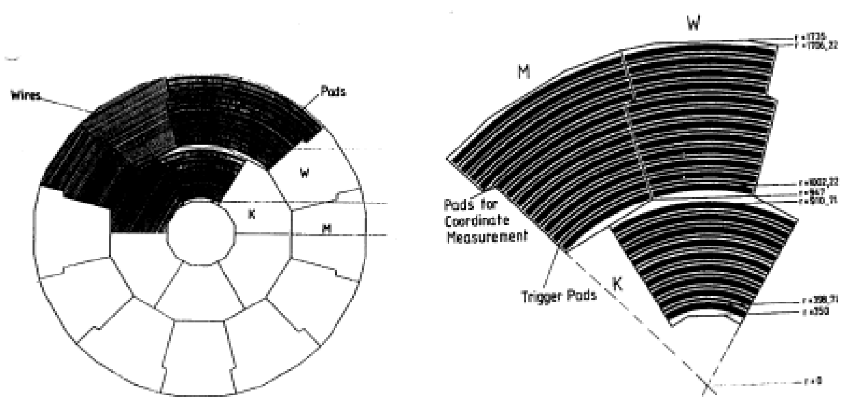

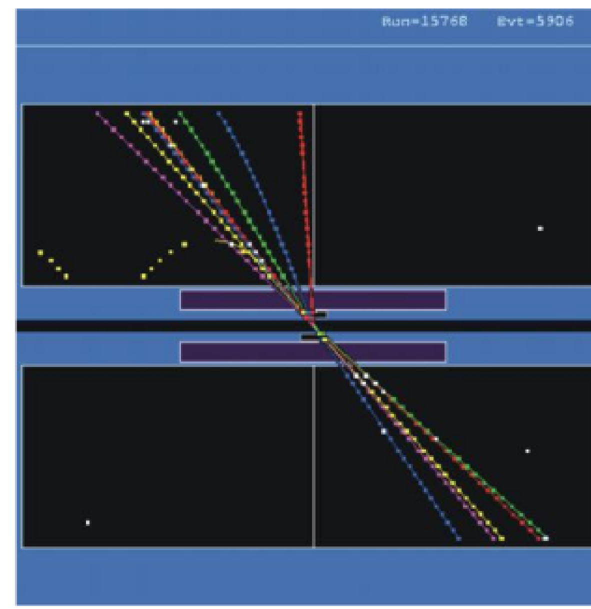

gute Auflösung in beiden Projektionen! $\sigma_z \sim 200\,\mu m$ (Driftzeit)
$\sigma_{r\phi} \sim 180\,\mu m$ (Pads)

Zeitprojektionskammer: ALICE am LHC

- Largest TPC:
  - Length 5m
  - Diameter 5m
  - Volume 88m^3
  - Detector area 32m^2
  - Channels ~570 000
- High Voltage:
  - Cathode -100kV
- Material X_0
  - Cylinder from composite materials from airplane industry (X0= ~3%)

- B Field 0.5 T (L3 magnet)
- E Field 400 V/cm
- Gas gain 10^4
- Position resolution ≈ 250 μm

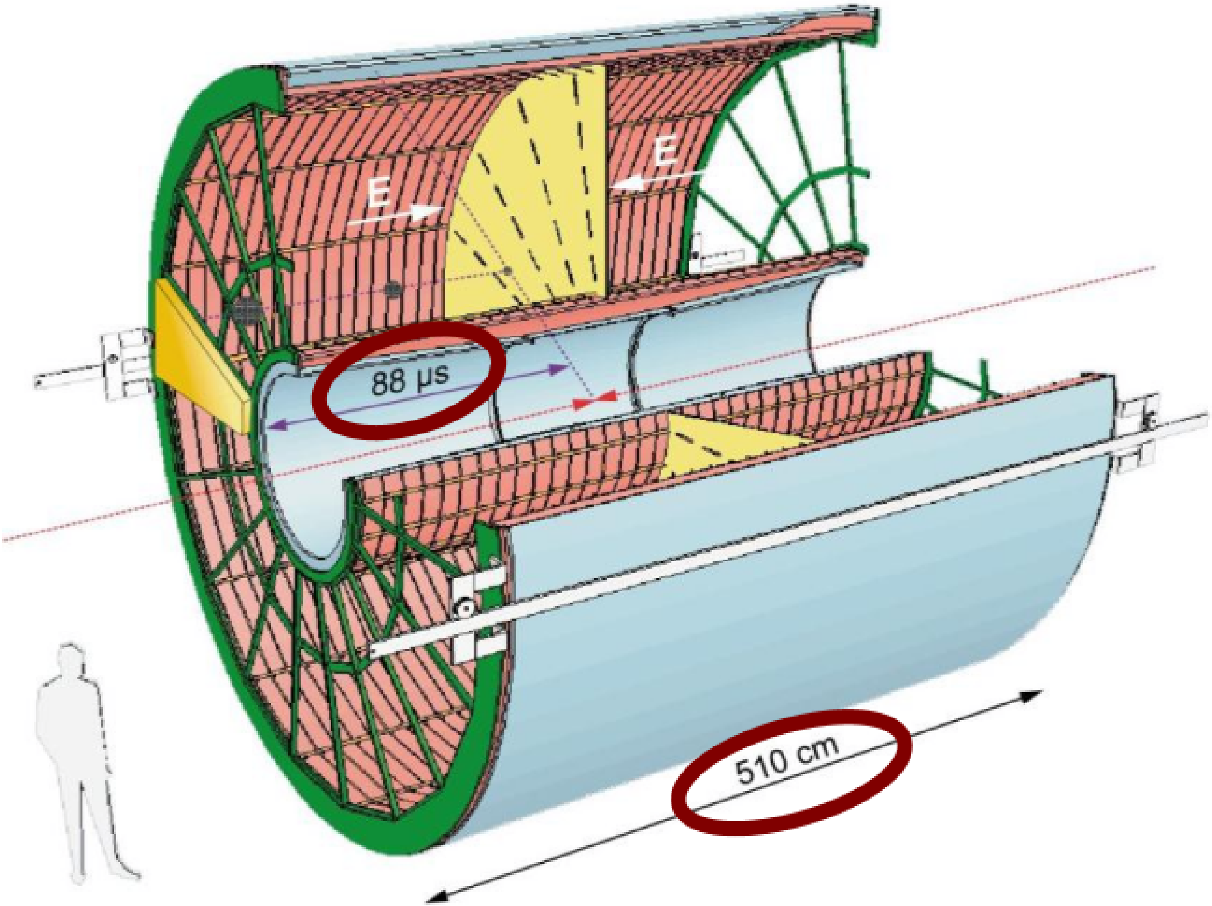

ALICE-TPC am LHC

View inside the ALICE TPC

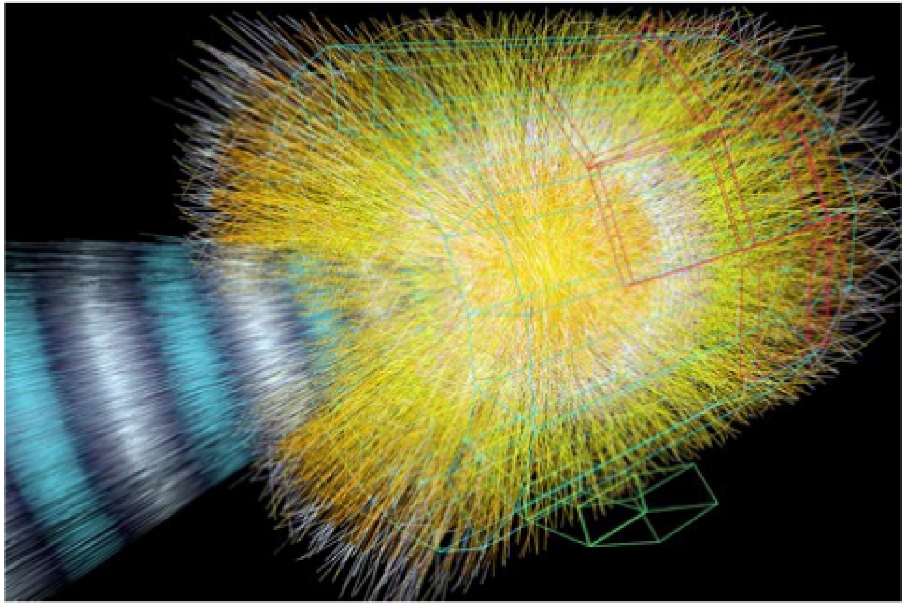

Mikrostrukturierte Gasgefüllte Detektoren

Try to overcome problems of e.g. MWPC like limited rate capability

→ Reduce size of sensitive cells

MICROMEGA

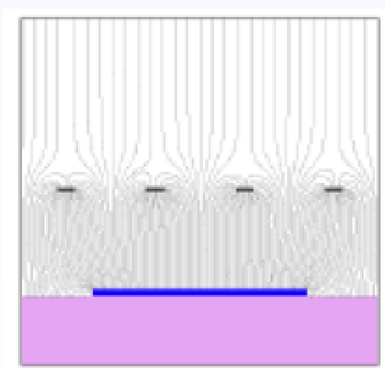

parallel plate

MicroMeshGasdetector

MSGC

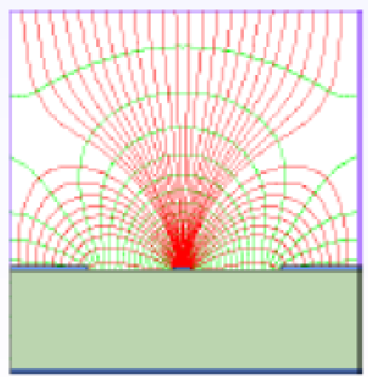

strip

MicroStripGasChamber

GEM

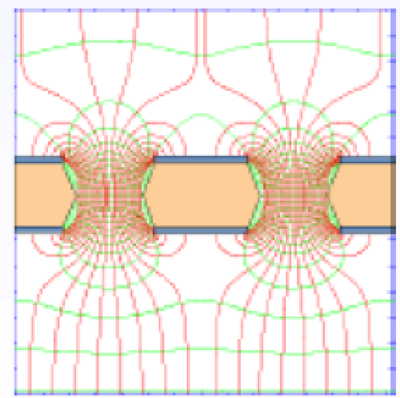

hole

GasElectronMultiplier

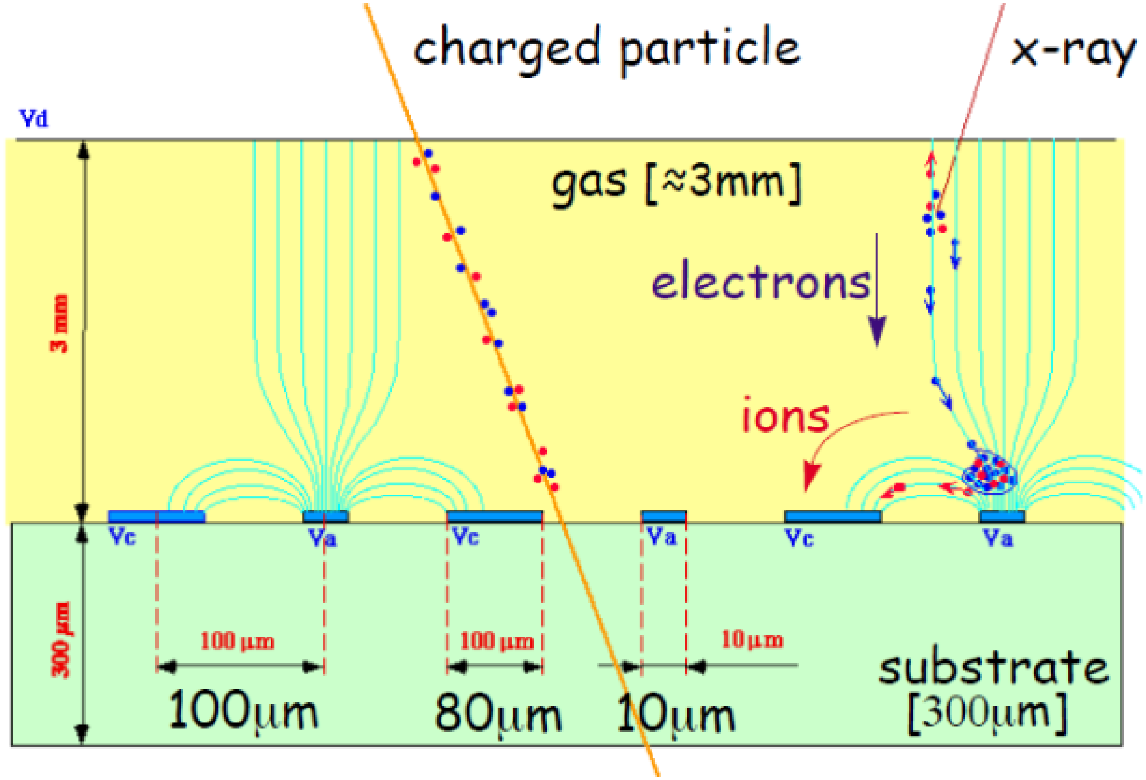

Advantages:

- Very precise and small anode/cathode structures can be produced with lithographical methods. Thus very good position resolution is possible.
- MSGC provide high mechanical stability
- small drift distance for ions, thus high rate capability.

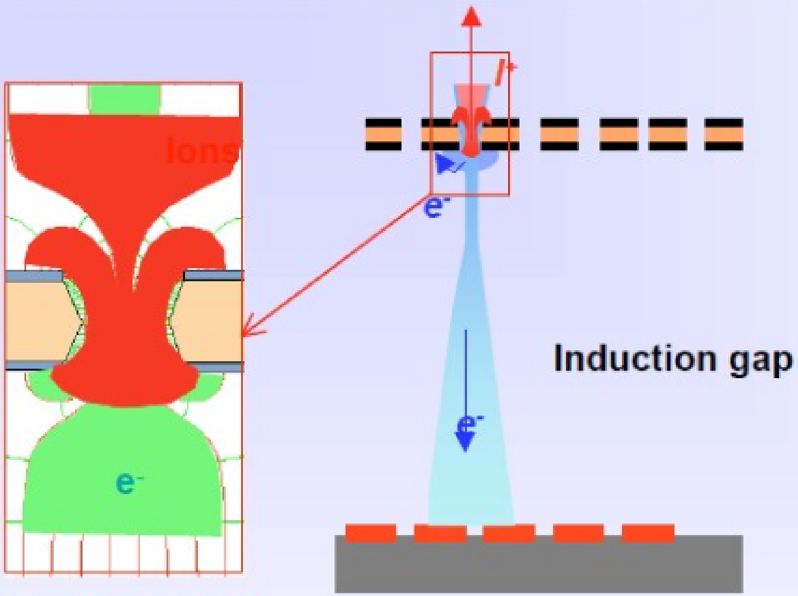

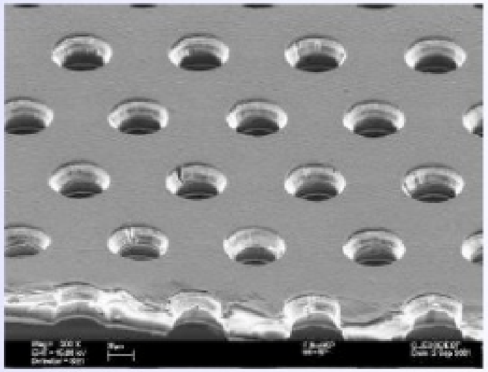

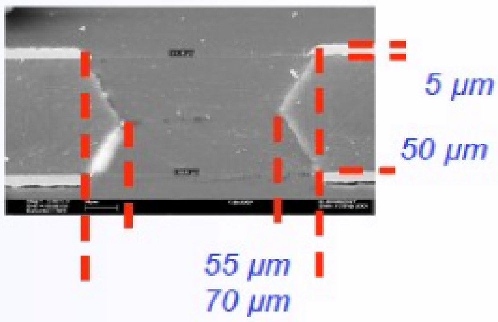

Thin, metal coated polyimide foil perforated with high density holes.

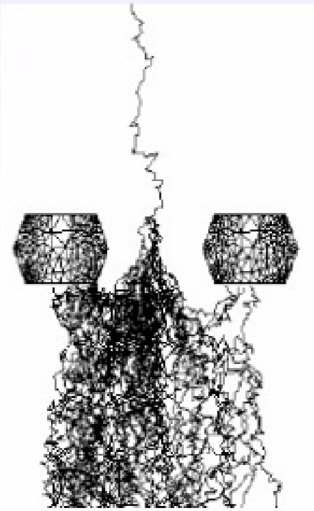

Electrons are collected on patterned readout board.
A fast signal can be detected on the lower GEM electrode for triggering or energy discrimination.
All readout electrodes are at ground potential.
Positive ions partially collected on the GEM electrodes.

Mikrostrukturierte Gasgefüllte Detektoren:GEM

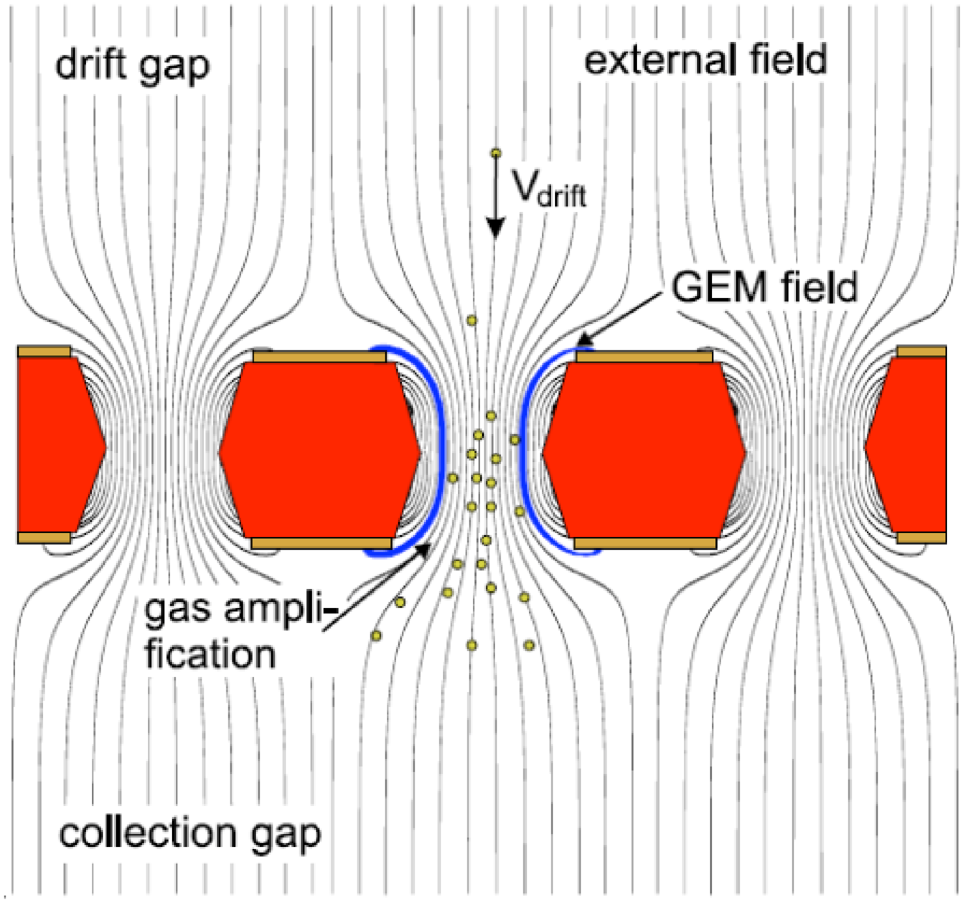

P. Cwetanski, thesis, Heidelberg

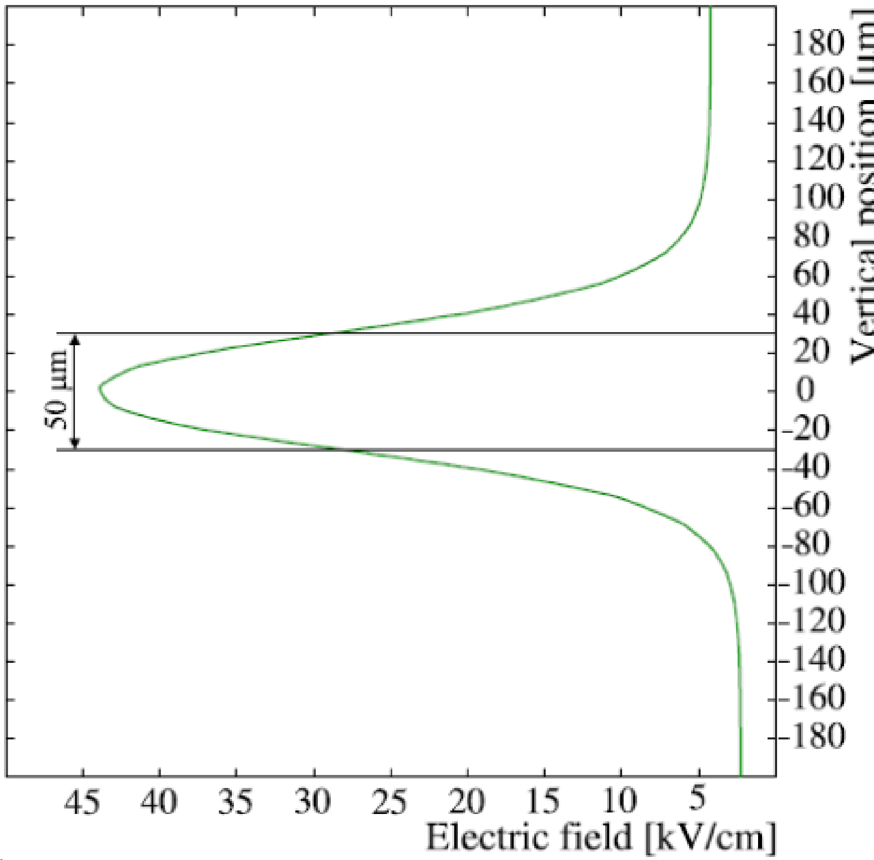

For a voltage between the GEM foils of 360 V the E-Field inside the gap reaches very high values, which cause gas amplification.